Electronic Structure

PAPER

Many-body van der Waals interactions in wet MoS_2 surfaces

Xuecheng Shao[1,*], **Alina Umerbekova**[1], **Kaili Jiang**[1] **and Michele Pavanello**[1,2,*]

[1] Department of Chemistry, Rutgers University, Newark, NJ 07102, United States of America
[2] Department of Physics, Rutgers University, Newark, NJ 07102, United States of America
[*] Authors to whom any correspondence should be addressed.

E-mail: xuecheng.shao@rutgers.edu and m.pavanello@rutgers.edu

Keywords: van der Waals, MoS_2, DFT, embedding, many-body

RECEIVED
5 February 2022

REVISED
8 March 2022

ACCEPTED FOR PUBLICATION
24 March 2022

PUBLISHED
18 April 2022

Abstract

Many-body dispersion (MBD), and generally many-body correlation effects, have emerged in recent years as key contributions to intermolecular interactions in condensed phases affecting nearly every field in the molecular sciences. *Ab initio* electronic structure methods are the golden standard of material science but unfortunately they are too computationally expensive for evaluating MBD in such complex systems as liquid–solid interfaces. In this work, we leverage subsystem time-dependent DFT's rigorous decomposition of the system's response function into subsystem contributions to evaluate the effect of many-body correlation effects (which include dispersion) for each water molecule in a model of wet MoS_2 surface. The optical spectra and and to a lesser extent the effective molecular C_6 coefficients display a dependence on a handful of order parameters describing the liquid as well as the distance and orientation of the molecules with respect to the surface. Overall, we provide an unprecedented, granular analysis of many-body correlation effects for wet MoS_2 which will be useful for developing more approximate models, such as force fields and other multi-scale methods for water–surface interactions.

1. Introduction

Rational design of materials hinges upon the ability of computational models to provide accurate predictions of materials properties. From light–matter interaction [1–4] to mechanical properties [5–7], computational models are becoming accurate enough to be a structural part of materials engineering [8]. Due to the central role of electronic structure in determining materials properties, *ab initio* electronic structure methods, such as density functional theory (DFT) are particularly relevant.

Despite the exciting and important advances in DFT made in recent years in terms of software implementations [9–15] as well as density functional development [16, 17], materials interfaces remain a very challenging type of system. This is because the nature of the electronic structure in the two materials at the interface may be very different and a single computational method may not be able to deliver the needed accuracy, or not be computationally feasible due to algorithm complexity.

Among those electronic properties that are difficult to characterize and predict is many-body dispersion (MBD) [18–21]. It has been shown that MBD plays an important role in the complex physics governing interfaces [22, 23], as well as the structure of liquids [24] and molecular crystals [21, 25]. Even though the currently-available, low-complexity methods for inferring upon MBD are semiempirical in nature, they have already shed light on the complex electron and nuclear dynamics that arises when they are taken into account [20].

Dispersion interactions can be accounted for in DFT simulations using an array of methods [26–29], which also include efficient *ab initio* algorithms based on RPA [30–33]. Standard time-dependent DFT (TDDFT) is capable to predict C_6 coefficients of atoms and jellium spheres accurately [34], when approaching more complex materials, such as fullerenes, the explicit inclusion of MBD leads to effective C_6 coefficients of larger magnitude than predicted from standard methods [30]. A similar effect is found when self-consistent MBD-including methods are applied to molecule–metal and semiconducting surfaces interactions [22, 23, 35]. Despite these notable advances and applications, the development of quantitative electronic structure methods

capable of characterizing MBD and generally van der Waals interactions in complex systems is still active and needed to address open questions, especially for interfaces, from optoelectronics to tribology [36–38].

Modeling water-2D materials interfaces is a complex task and yet very important from the materials engineering prospective. Particularly, water on MoS_2 and graphene are interesting cases where it is known that the properties of the interface cannot be inferred from studies of simplified models comprising of single molecules adsorbed on the surface. For example, when single water molecules interact with these surfaces, the H-atom points toward the surface. However, differences arise when there are layers of water [39]. Even though it is known that edges play a significant role and are responsible for the large part of reactivity [40, 41], in this work we focus on the interaction of water with basal plane, which is important for tribology (lubrication) [38, 42–45] and adsorption studies for catalysis and sensing, among others fields [46].

We focus specifically on the surface enhancement of the van der Waals interactions involving water molecules near a surface of MoS_2. The main goal being to characterize the size of MBD by computing the effective molecular C_6 coefficients in two ways: (1) a 'coupled' way, where the molecules and the surface are allowed to mutually polarize each other. The mutual polarization is at the core of MBD when the polarization is computed at imaginary frequency, and screening when it is computed for real values of the frequency. (2) An 'uncoupled' way [23, 47–59] where surface and molecules are not allowed to mutually polarize. We will more clearly discuss these two types of calculations in the next section. So far, no studies have quantified the effects of MBD on the size of molecular C_6 coefficients for wet MoS_2 interfaces. We fill this gap in this work, specifically looking into how the water's C_6 coefficients are affected by MBD arising from the interactions among waters and between them and MoS_2.

This paper is organized as follows. In section 2, we first provide the necessary theoretical framework underlying our simulations. In section 3 we briefly list the computational details of the simulations. In section 4, we present and discuss the results, including a detailed analysis of the correlations between the computed molecular response properties and order parameters of the liquid. We then draw conclusions in section 5.

2. Theoretical and computational considerations

In this work we use subsystem TDDFT (sTDDFT) [53, 60–63] to infer on the enhancement of the van der Waals interactions in liquid water when it is nearby a MoS_2 surface. There are several advantages for employing sTDDFT compared to regular TDDFT. First is the computational scaling of the simulations. And second is the ability to decompose the dynamic response of the system into subsystem contributions which have clear physical interpretation.

The computational scaling of sTDDFT simulations is much reduced compared to regular TDDFT because sTDDFT is based on subsystem DFT (sDFT), which treats all non-bonded fragments (in this case each of the water molecules and the MoS_2 surface) as subsystems. A subsystem Hamiltonian is associated to each subsystem, diagonalized in a reduced basis whose spatial extent is close to the region where the subsystem electron density is non-zero, i.e., a monomer basis set [13, 64, 65]. The resulting algorithm is massively parallel as the subsystem Hamiltonian diagonalization can take place independently. See section 3 for further details.

Perhaps the most important advantage of using sTDDFT is that one can infer on properties of the single subsystems as they interact dynamically with the subsystems in their environment. This is in contrast with regular TDDFT where only the properties of the entire system are available. We remark here that sTDDFT is not related to population analyses, instead it constitutes an alternative way to solve for the electronic structure, a way that focuses on the single non-bonded fragments in the system [49, 66–68].

In sDFT, the total electron density $\rho(\mathbf{r})$ is given as a sum of subsystem densities $\{\rho_I(\mathbf{r})\}$,

$$\rho(\mathbf{r}) = \sum_I^{N_S} \rho_I(\mathbf{r}), \tag{1}$$

where N_S is the number of the subsystems. The subsystem electron densities are determined for the ground state by minimizing the total energy functional,

$$E[\{\rho_I\}] = \sum_I^{N_S} E[\rho_I, v_{ext}^I] + E_{xc}^{nadd}[\{\rho_I\}] + T_s^{nadd}[\{\rho_I\}] + V_{Coul}[\{v_{ext}^I, \rho_I\}], \tag{2}$$

where the total external potential has been split into subsystem contribution, $v_{ext}(\mathbf{r}) = \sum_I v_{ext}^I(\mathbf{r})$ and we have introduced additional functionals: the non-interacting kinetic energy, T_s, the exchange–correlation, E_{xc} [69] (xc, hereafter), and the Coulomb interactions between the subsystems, V_{Coul}. The non-additive functionals are defined simply by

$$F^{\text{nadd}}[\{\rho_I\}] = F[\rho] - \sum_I F[\rho_I]. \tag{3}$$

The functional in equation (2) can be minimized variationally by solving the following coupled KS equations for each subsystem

$$-\frac{1}{2}\nabla^2\phi_i^I(\mathbf{r}) + \left(v_s[\rho_I](\mathbf{r}) + v_{emb}[\{\rho_I\}](\mathbf{r})\right)\phi_i^I(\mathbf{r}) = \varepsilon_i^I\phi_i^I(\mathbf{r}), \tag{4}$$

where $v_s(\mathbf{r})$ is the KS potential of the isolated subsystem evaluated with the embedded subsystem electron density, ρ_I. The embedding potential, $v_{\text{emb}}(\mathbf{r})$, is a functional of all the subsystem electron densities and stems from the functional derivative of all the subsystem non-additive terms in the energy functional equation (2).

The response to external time-dependent perturbations in sTDDFT is characterized by subsystem linear response functions which make up the response of the full system, namely, $\chi(\mathbf{r},\mathbf{r}',\omega) = \sum_I \chi_I(\mathbf{r},\mathbf{r}',\omega)$ [61, 63]. Each subsystem response function can be recovered solving for a Dyson equation involving the 'uncoupled' and 'coupled' subsystem response function, χ_I^u and χ_I, respectively. Dropping the arguments of the response functions in a short-hand notation for the spatial integrals involved,

$$\chi_I = \chi_I^u + \sum_J \chi_I^u K_{IJ}\chi_J, \tag{5}$$

where the kernel is given by [60]

$$K_{IJ}(\mathbf{r},\mathbf{r}') = \frac{1}{|\mathbf{r}-\mathbf{r}'|} + f_{\text{xc}}[\rho](\mathbf{r},\mathbf{r}') + \left(f_{Ts}[\rho](\mathbf{r},\mathbf{r}') - \delta_{IJ}f_{Ts}[\rho_I](\mathbf{r},\mathbf{r}')\right). \tag{6}$$

In the above equation, we have already assumed that we will invoke the so-called adiabatic approximation whereby the frequency dependence of the xc and T_s kernels is ignored. The adiabatic approximation has been characterized in several works for the xc [70–73] as well as the kinetic energy [74, 75] kernels. Therefore, kernels are here assumed to be the second functional derivative with respect to the electron densities displayed in their arguments. Further, we have assumed that we use the same xc functional for the subsystem-additive and non-additive parts of the xc energy functional in equation (2). The term in parentheses stems from the non-additive kinetic energy functional which retains the non-additive structure only for the subsystem-diagonal kernel elements (K_{II}) [52, 60] (hence the presence of the Kronecker delta).

The uncoupled subsystem response functions, χ_I^u, encapsulate the response of the subsystem as if the other subsystems in the environment were frozen in their ground state electron densities. One can think of them as closed-subsystem response functions ('closed' to the energy transfer) as opposed the open-subsystem response functions which are given by the 'coupled' response functions [63].

C_6 coefficients, subject of this work, are computed directly from the subsystem dynamical dipole polarizabilities, $\alpha_I(\omega)$, which are derived from the response functions, $\alpha_I(\mathbf{r},\mathbf{r}',\omega) = \mathbf{r}\chi_I(\mathbf{r},\mathbf{r}',\omega)\mathbf{r}'$. Dynamical polarizabilities naturally also come in two flavors, coupled and uncoupled, depending on whether they are computed from the coupled or the uncoupled subsystem response functions. To compute the C_6 coefficients, we first need to trace the dynamical polarizability over Cartesian directions, to retrieve the dynamical dipole polarizability tensor (we only use the *zz* component, i.e., the component that is perpendicular to the MoS_2 surface plane) and then we perform the following integral,

$$C_6^{IJ} = \frac{3}{\pi}\int_0^\infty \alpha_{zz,u}^I(\mathrm{i}\omega)\alpha_{zz,c}^J(\mathrm{i}\omega)\mathrm{d}\omega. \tag{7}$$

In the above equation, the c and u labels stand for coupled and uncoupled (recall the definition in equation (5)). Also note that the dynamical dipole polarizabilities are evaluated for imaginary frequencies [76, 77], or equivalently, rather than computing them as Fourier transforms of the time-dependent polarizabilities one can use Laplace transform instead [78].

The reason why the C_6 coefficient features one coupled and one uncoupled dynamic dipole polarizability has to do with the definition of van der Waals interactions in the context of sTDDFT. We showed [79, 80] that dispersion interactions as well as more generally van der Waals interactions are simply the non-additive correlation energy which is formally given by

$$E_c^{\text{nadd}} = -\frac{1}{2\pi}\sum_{IJ}\int d1d1'd2d2'\int_0^\infty \mathrm{d}\omega\frac{\chi_I^u(1,1')K_{IJ}(1',2)\chi_J(2,2')}{|\mathbf{r}_{12'}|}, \tag{8}$$

where we have used a short-hand notation for the spatial variables and have also omitted the coupling strength integration for sake of simplicity. We refer the reader to references [23, 79, 80] for additional details. When the kernel K_{IJ} in the above equation (see also equation (6)) is truncated to only include the Coulomb interaction,

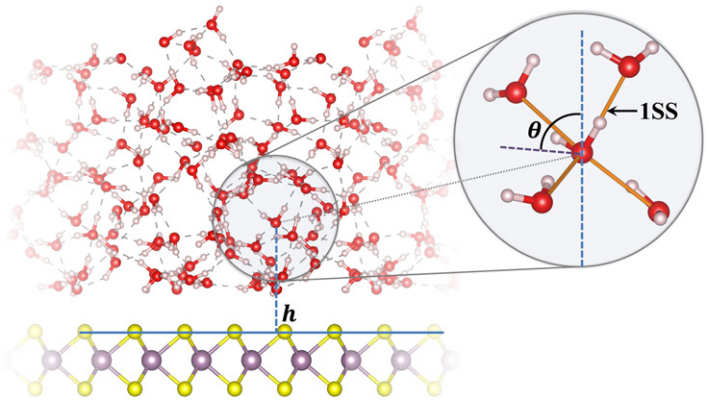

Figure 1. Depiction of the water–MoS_2 interface system considered in this work. See text for details. Structure files available in the supplementary materials [89].

one obtains the so-called RPA approximation [81–83] which is needed to define dispersion interactions and the C_6 coefficient formula in equation (7).

Thus, we can characterize the surface 'many-body' effects on the C_6 coefficients by computing the fully coupled C_6 coefficient from equation (7), and compare it to the uncoupled C_6^u which is recovered by utilizing both uncoupled response functions in equation (7). The comparison of these two quantities can be represented by their difference,

$$\Delta C_6 = C_6 - C_6^u, \tag{9}$$

giving a measure of the enhancement of the van der Waals interaction given by the dynamical coupling of the response functions of the subsystems. To simplify our analysis, we only compute the diagonal coefficients, $C_6 = C_6^{\mathrm{II}}$. This is common practice and is done to reduce the number of computed coefficients, is practical in nature without compromising on the scientific soundness of the results.

3. Computational details

All calculations have been carried out with eDFTpy [84], an all-Python software that implements sDFT and sTDDFT. The Kohn–Sham engine to compute the electronic structure of each subsystem is Quantum ESPRESSO version 6.5 [85] which was coupled to eDFTpy by the QEpy API [86]. QEpy is a Python version of Quantum ESPRESSO that allows direct access to wavefunctions, electron density and diagonalization drivers. QEpy also gives the possibility to impose custom external potentials to Quantum ESPRESSO. This is a key functionality for implementing sDFT.

The TDDFT equations were solved by real-time subsystem TDDFT also implemented in eDFTpy. We use ce-TDDFT as the TDDFT solver by Ceresoli and coworkers [48, 87] which was adapted with a Python API for its integration in eDFTpy.

Large scale simulations [88] show that the structure of liquid water on the surface of MoS_2 is heavily influenced by the interactions with the surface. The bulk water structure is only recovered at about 10 Å above the surface. In addition, the first layer of water on MoS_2 avoids the S top sites. Therefore, we chose a model system containing 64 water molecules sandwiched by MoS_2 monolayer slabs separated by 20 Å. See figure 1 for a pictorial view of the model system. Each water molecule and the MoS_2 monolayer constitute a subsystem. While the simulation cell dimensions are $a = 12.72$ Å, $b = 11.02$ Å, $c = 23.27$ Å, the subsystems cell dimensions are massively reduced. The water subsystems used cells with a, b and c reduced by 40%, 30% and 65%, respectively, compared to the simulation cell of the supersystem. This yielded a reduction in terms of employed plane waves for the diagonalization of the subsystem Hamiltonians of 85% for each water molecule. The MoS_2 subsystem utilized a simulation cell with c reduced by 40% compared to the physical simulation cell resulting in a 40% reduction of the number plane waves used for the diagonalization of its Hamiltonian.

We consider two geometries each containing 64 water molecules. The xyz files are deposited in the supplementary materials [89]. The structures considered here were optimized without the inclusion of MBD. Therefore, we acknowledge that our results and conclusions may carry a bias. The determination of the relaxed structures including MBD is out of the scope of this paper and will be the subject of future work.

We use the PBE [90] xc and the revAPBEK [91] non-additive kinetic energy functionals, the GBRV ultrasoft pseudopotentials [92] and a plane wave cutoff of 40 Ry for the subsystem wavefunctions, 400 Ry for the subsystem electron density and 200 Ry for the total electron density when it is represented on the full

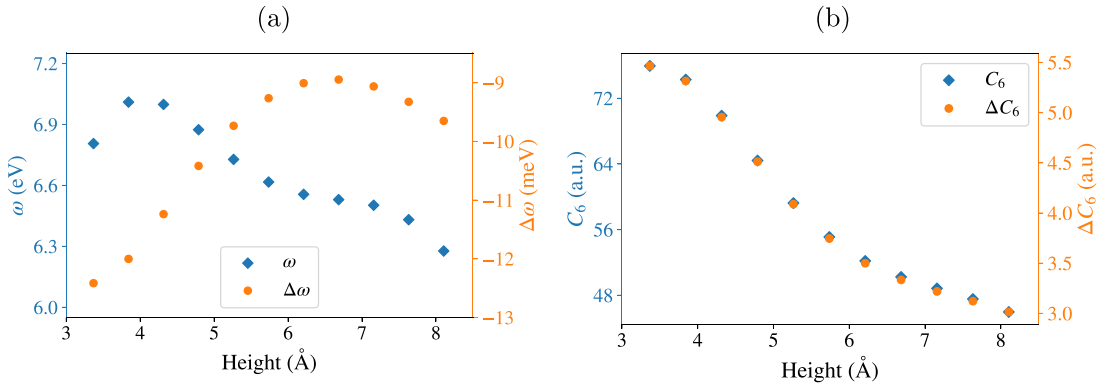

Figure 2. First excitation energy, ω^{u}, from the response of water that is uncoupled to the surface response in inset (a) and effective uncoupled C_6^u coefficient in inset (b) of the water subsystems alongside their surface enhancements as a function of height (see h in figure 1). C_6 coefficients and enhancements are given in atomic units (Ha·a_0^6). The data was convoluted with Gaussians of width 1.5 Å, sampled every 0.5 Å.

(physical) simulation cell. The reciprocal space energy cut-off parameters were chosen to converge the total energy to within 1 kcal mol^{-1} separately for the additive and nonadditive energy (similar to what was shown in reference [93]). We additionally checked that the total energy during a sTDDFT real-time propagation was conserved well, oscillating by less than 10 meV and exposing no appreciable energy drift.

In figure 1, we also show the order parameters that we use for our analyses. The θ angle is the angle between the z axis (perpendicular to the surface plane) and the perpendicular to the planes defined by the three atoms of each water molecule. 1SS is a measure of the distance of the first solvation shell given by the average distance from one oxygen the closest four nearby oxygen atoms. h is the distance of an oxygen atom from the surface.

4. Results

In the following, we present results about each water molecule's C_6 coefficient and excitation energy both in the case when the underlying subsystem response functions are dynamically uncoupled to the surface (C_6^u and ω^{u}) as well as when they are coupled. We characterize the coupling by reporting the coupled-uncoupled shifts, ΔC_6 and $\Delta\omega$. These shifts are a measure of the dynamical many-body effects on the excitation energy as well as on the C_6 coefficients. The uncoupled quantities are computed by explicitly removing the coupling of the molecular subsystem response functions with the surface. Surface effects are still present in the uncoupled quantities because the ground state electron densities of the molecular subsystems are affected by the presence and interaction with the surface. We expect ΔC_6 and $\Delta\omega$ to be a proxy for the size of the coupling between excited states of the water molecules and the surface.

As we have showed before [23], molecules adsorbed on MoS_2 monolayers display enhanced effective C_6 coefficients due to the many-body nature of the molecular dynamic dipole polarizability (see equation (5) for the charge density response functions). For benzene at MoS_2 we predicted up to a 5% enhancement. The system in reference [23] was very simple, as it was comprised only of a single benzene molecule on the surface and only a few representative (symmetric) configurations were considered. Thus, recovering enhancement trends with respect to the molecule–surface distance was straightforward. In real life, however, systems are more similar to figure 1, where molecules arrange almost randomly on the surface. Thus, from the onset, we expect the trends to be more complicated and to require more nuanced analysis methods.

In figure 2, we present the trends of first excitation energy, ω, and its shift due to the inclusion of the dynamical interactions with the surface (i.e., including the surface in the many-body expansion of the response functions in equation (5)), $\Delta\omega$ in inset (a), and C_6 and its enhancement, ΔC_6, in inset (b) as functions of distance from the oxygen atom of the water subsystem to the closest plane of S atoms of the MoS_2 monolayer.

The trends in the figure are evident. For the excitation energy, the trends for the uncoupled excitation, ω^{u}, and the coupled–uncoupled shift are opposite, a phenomenon commonly witnessed for embedded systems [60]. The physical origin of such opposite behavior is rooted in the fact that embedding at the level of the ground state often does nothing more than adding confinement. The environment exerts pressure on the subsystem density resulting in the typical blue shift of the low-lying excitation energies. Thus, we expect ω^{u} to increase the closer the water molecule is to the surface.

However, we notice that the trend for ω^{u} inverts very close to the surface. The reason for such inversion is that water molecules in the layer closest to the MoS_2 surface couple strongly with the surface already at the ground state level. Their optical spectra are affected by the fact that their electron density is heavily influenced

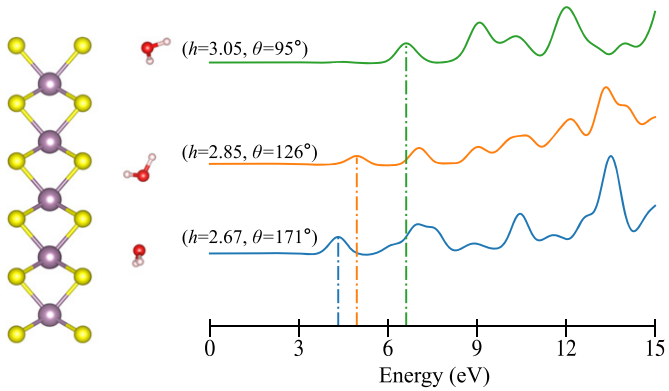

Figure 3. The spectrum of the closest three water molecules to the surface in our model. Each features different height (h) and angle (θ) values.

by the short range interactions with the surface having the effect of abruptly red-shifting the first excitation of water. To give an idea of such an effect, we show in figure 3 what happens to those water molecules that are very close, directly adsorbed to the MoS_2 surface. For the molecules directly in contact to the surface, the first excitation energy is severely red shifted compared to the liquid. Liquid water's first excitation energy is 6–6.5 eV when it is computed with the PBE xc functional [93, 94], thus we note that the molecule closest to the surface experiences a red shift of more than 2 eV compared to the liquid!

We note that PBE xc functional has the tendency of red shifting the spectral features in comparison to the experiment as noted in prior works [93, 94] and in several reviews [95]. However, the PBE results are expected to provide correct overall trends.

Going back to figure 2, we notice that the general trend for $\Delta\omega$ is opposite compared to ω^{u}. Such a trend can be explained because the excitation energy shift is related to excitonic couplings between the molecules and the surface. We remark that $\Delta\omega$ is fairly small in size, only a few tens of meV. This is to be expected because the excitonic couplings between the localized, first excitation of water and the excitations in the MoS_2 surface are weak. We will return to this point later.

The trends for the C_6 coefficients are, instead, much more pronounced. Both C_6^u and ΔC_6 increase in size as the water molecules are closer to the surface. Particularly, in comparison to the excitation energy shift, the ΔC_6 contribution to the total, coupled C_6 is orders of magnitudes larger, peaking at 8% for molecules close to the surface and tapering off to about 6% for further-away molecules. We explain the trend by noting that the excitation energies are given by poles of the subsystem response function for real values of the frequency, $\chi_I(\omega)$. The C_6 coefficients, instead, depend on the response functions evaluated for imaginary frequencies, $\chi_I(\mathrm{i}\omega)$. Thus, because all the excitations lie on the real axis, the C_6 values will be affected by the molecule–surface couplings of all the excited states. Molecular excited states become more and more delocalized the higher up in energy they lie. A stronger delocalization leads to a stronger molecule–surface coupling which leads to a stronger enhancement to the C_6 coefficients. On the flip side, due to their dependence on all the excited states of the molecules, we also expect the C_6 coefficients to display a weaker correlation to the geometrical order parameters of the liquid and the interface.

In figure 4 we report the optical spectrum (related to the dipole polarizability at real frequency) and the dipole polarizability at imaginary frequency. From the figure it can be appreciated the different levels of enhancement (and depletion) that take place for the two quantities. First, we notice that the optical spectrum up to 5 eV is nearly identical whether the water molecule's spectrum is computed with the one-body, uncoupled response function, χ_I^u, or with a many-body, fully coupled response function. This hints to the fact that the localized, first excitation in the water molecules does not engage in strong excitonic couplings with the other water molecules nor with the surface. The intensities are quite different for the higher lying excited states. Inspecting the one-body vs many-body spectra for excitation energies larger than 5 eV, we note that the one-body peak intensities are much reduced compared to the many-body ones. In addition, we see that if the water response function is allowed to couple with the surface response function, the peak intensities of high lying states are increased (see, e.g., the peaks in the range 5–20 eV). Above 20 eV, the situation is reversed.

The above considerations for the optical spectra, completely explain the trends witnessed for the dynamic dipole polarizability in inset (b) of figure 4. The decay of α_{zz}^I as a function of $\mathrm{i}\omega$ is due to the fact that the poles of the dynamic polarizability are all on the real frequency axis as explained before. Thus, the enhancement of the dynamic polarizability in inset (b) of figure 4 is fully explained.

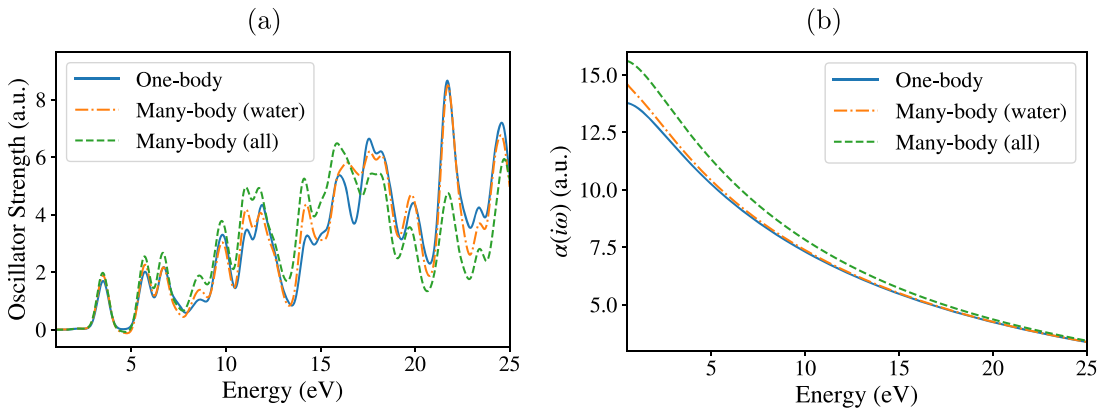

Figure 4. (a) Optical spectra of one selected water molecule close to the MoS_2 surface. Spectra are derived from the following response functions: χ_I^u (one-body), $\chi_I^u + \sum_{J\in\text{water}}\chi_I^u K_{IJ}\chi_J$ (many-body (water)) and $\chi_I^u + \sum_{J\in\text{water}}\chi_I^u K_{IJ}\chi_J + \chi_I^u K_{Is}\chi_s$ where χ_s is the response function of the MoS_2 monolayer (many-body (all)). (b) Dynamic dipole polarizability along the z axis, $\alpha_{zz}^I(i\omega)$, derived from the response functions mentioned before.

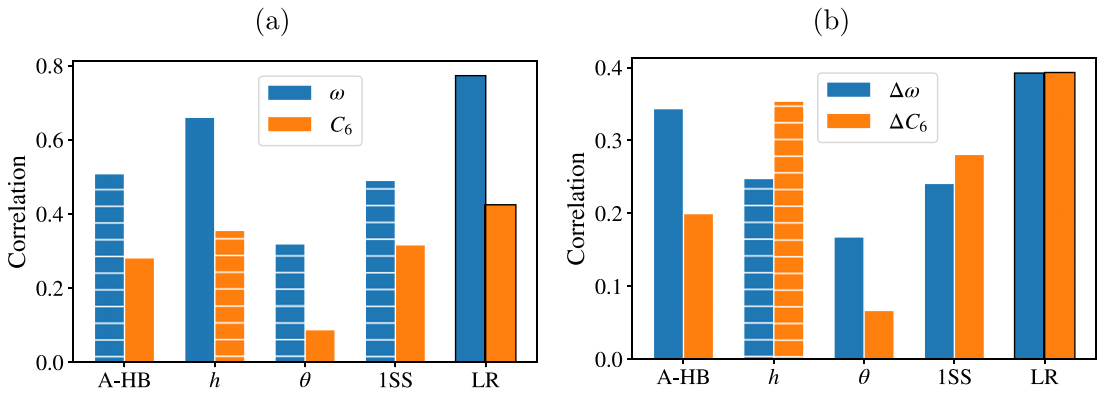

Figure 5. Bar chart of correlation coefficients against several order parameters (see figure 1 and text for details) of (a) uncoupled ω^u and C_6^u (see text for definitions) and (b) surface enhancements, $\Delta\omega$ and ΔC_6. Regression of ω^u and C_6^u and their shifts with all the order parameters is indicated by LR which stands for linear regression (see supplementary materials for details [89]).

A question may arise regarding the fact that the intensity of the one-body spectrum increases for higher-lying excitations. The answer is simple and recalls concepts from the physics of semiconductors [96]. Switching on excitonic couplings between the water molecules and with the surface has the effect of increasing the transition dipole of the excited states at low frequencies. Because the coupling term of the coupled response function, $\sum_J \chi_I^u K_{IJ}\chi_J$, must be associated with an overall zero sum rule, the high-lying excited states will witness a decrease in their intensity. We analyzed such a behavior before for liquid water [93].

Figures 2 and 3 reveal correlation between the computed quantities and the distance of the molecules to the surface. However, the orientation of the water molecules should also, in principle, factor in, making it difficult to attribute the trends exclusively on the molecule–surface distance. To infer on the correlation of the excitation energy as well as the C_6 coefficients on the structure of the interface, in figure 5 we present the correlation coefficients, determined in the usual way

$$C_{XY} = \frac{\sigma_{XY}}{(\sigma_{XX}\sigma_{YY})^{\frac{1}{2}}}, \tag{10}$$

where $\sigma_{XY} = \sum_i (X_i - \bar{X})(Y_i - \bar{Y})$, between the water molecules' C_6 and ω values and several order parameters which we described in the computational details section 3.

A general observation is that all except the correlation between ω^u and h are below 0.6. This means that either the correlation of ω^u and C_6^u with the order parameters of the system is non-linear in nature or on average is, simply put, poor. The second most important order parameter is the number of hydrogen bonds accepted (A-HB) which is followed by the size of the first solvation shell (1SS). The correlations in this work for the

optical spectrum of water confined at the interface with MoS_2 are similar to those drawn for the optical spectrum of bulk liquid water [93] where it was found that the number of hydrogen bonds and the characteristics of the first solvation shell correlate the most with the first excitation energy of the water molecules.

To understand if the order parameters considered are capable of capturing the overall trend in the computed quantities, we carried out linear regressions of four computed quantities against the entire data set, which is indicated by LR in figure 5. We notice that LR gives a value of 0.78 for ω^{u} and smaller values for the other three quantities. This confirms that the first excitation energy can be reproduced by a linear function of the order parameters. Conversely, the C_6^u coefficients and the shifts do not correlate enough with the given order parameters, instead, as seen in figure 2, they only weakly correlate with the distance to the surface. Additional details can be found in the supplementary materials [89]. We should remark that the analysis relies exclusively on linear regressions and the data set available is quite small. It is therefore possible that there is a non-linear relation between the C_6^u coefficients or the shifts and the order parameters. We do not investigate this question in this work and we reserve it for a follow-up study.

5. Conclusions

To conclude, for the first time to date, we report computed effective molecular C_6 coefficients as well as optical spectra of water molecules in a water–MoS_2 interface with an accurate, *ab initio* electronic structure method. We found that the C_6 coefficients of water are strongly enhanced by the coupling of the molecular excitations to the surface bands reaching close to 8% enhancement for those molecules directly adsorbed to the surface and tapering off to about 6% for further-away molecules. The trends show correlation of the first excitation energy of the water molecules as well as the molecular C_6 coefficients with respect to the distance of the molecules to the surface, and to a lesser extent to the details of the structure of the liquid (e.g., the hydrogen bond network and the size of the first solvation shell). Overall, we conclude that for water on MoS_2, MBD in the form of surface enhanced C_6 coefficients are important and must be accounted for in accurate simulations of this system.

Acknowledgments

This work is supported by the US Department of Energy, Office of Basic Energy Sciences, under Award Number DE-SC0018343. We thank the Office of Advanced Research Computing at Rutgers for providing access to the Amarel cluster.

Data availability statement

The data that support the findings of this study are openly available at the following URL/DOI: 10.5281/zenodo.5971766.

ORCID iDs

Michele Pavanello https://orcid.org/0000-0001-8294-7481

References

[1] Andreussi O, Caprasecca S, Cupellini L, Guarnetti-Prandi I, Guido C A, Jurinovich S, Viani L and Mennucci B 2014 *J. Phys. Chem.* A **119** 5197
[2] Moore J E and Jensen L 2016 *J. Phys. Chem.* C **120** 5659
[3] Rossi T P, Winther K T, Jacobsen K W, Nieminen R M, Puska M J and Thygesen K S 2017 *Phys. Rev.* B **96** 155407
[4] Foerster B, Spata V A, Carter E A, Sönnichsen C and Link S 2019 *Sci. Adv.* **5** aav0704
[5] Lu G, Kioussis N, Bulatov V V and Kaxiras E 2000 *Phys. Rev.* B **62** 3099
[6] Aguado A and López J M 2013 *J. Phys. Chem. Lett.* **4** 2397
[7] Shin I, Ramasubramaniam A, Huang C, Hung L and Carter E A 2009 *Phil. Mag.* **89** 3195
[8] Carter E A 2008 *Science* **321** 800
[9] Shao X, Jiang K, Mi W, Genova A and Pavanello M 2021 *WIREs: Comput. Mol. Sci.* **11** e1482
[10] Giannozzi P *et al* 2020 *J. Chem. Phys.* **152** 154105
[11] Ehlert C and Klamroth T 2020 *J. Comput. Chem.* **41** 1781
[12] Sun Q *et al* 2018 PySCF: the python-based simulations of chemistry framework *Wiley Interdiscip. Rev. Comput. Mol. Sci.* **8** e1340
[13] Mi W, Shao X, Genova A, Ceresoli D and Pavanello M 2021 *Comput. Phys. Commun.* **269** 108122
[14] Unsleber J P, Dresselhaus T, Klahr K, Schnieders D, Böckers M, Barton D and Neugebauer J 2018 *J. Comput. Chem.* **39** 788
[15] Shao Y *et al* 2006 *Phys. Chem. Chem. Phys.* **8** 3172

[16] Sun J, Ruzsinszky A and Perdew J P 2015 *Phys. Rev. Lett.* **115** 036402
[17] Baer R, Livshits E and Salzner U 2010 *Annu. Rev. Phys. Chem.* **61** 85
[18] Tkatchenko A, DiStasio R A, Car R and Scheffler M 2012 *Phys. Rev. Lett.* **108** 236402
[19] Hermann J, DiStasio R A and Tkatchenko A 2017 *Chem. Rev.* **117** 4714
[20] Ambrosetti A, Ferri N, DiStasio R A and Tkatchenko A 2016 *Science* **351** 1171
[21] DiStasio R A, Gobre V V and Tkatchenko A 2014 *J. Phys.: Condens. Matter* **26** 213202
[22] Ferri N, DiStasio R A, Ambrosetti A, Car R and Tkatchenko A 2015 *Phys. Rev. Lett.* **114** 176802
[23] Umerbekova A and Pavanello M 2020 *Int. J. Quantum Chem.* **120** e26243
[24] DiStasio R A, Santra B, Li Z, Wu X and Car R 2014 *J. Chem. Phys.* **141** 084502
[25] Gobre V V and Tkatchenko A 2013 *Nat. Commun.* **4** 2341
[26] Becke A D and Johnson E R 2007 *J. Chem. Phys.* **127** 154108
[27] Becke A D and Johnson E R 2005 *J. Chem. Phys.* **122** 154104
[28] Caldeweyher E, Bannwarth C and Grimme S 2017 *J. Chem. Phys.* **147** 034112
[29] Caldeweyher E, Ehlert S, Hansen A, Neugebauer H, Spicher S, Bannwarth C and Grimme S 2019 *J. Chem. Phys.* **150** 154122
[30] Ruzsinszky A, Perdew J P, Tao J, Csonka G I and Pitarke J M 2012 *Phys. Rev. Lett.* **109** 233203
[31] Eshuis H and Furche F 2011 *J. Phys. Chem. Lett.* **2** 983
[32] Eshuis H, Yarkony J and Furche F 2010 *J. Chem. Phys.* **132** 234114
[33] Furche F and Van Voorhis T 2005 *J. Chem. Phys.* **122** 164106
[34] Tao J, Perdew J P and Ruzsinszky A 2011 *Proc. Natl Acad. Sci. USA* **109** 18
[35] Maurer R J, Ruiz V G and Tkatchenko A 2015 *J. Chem. Phys.* **143** 102808
[36] Leung K 2020 *Phys. Chem. Chem. Phys.* **22** 10412
[37] Di Liberto G and Pacchioni G 2021 *J. Phys.: Condens. Matter* **33** 415002
[38] Zhao X and Perry S S 2010 *ACS Appl. Mater. Interfaces* **2** 1444
[39] Köhler M H and Gavazzoni C 2019 *J. Phys. Chem.* C **123** 13968
[40] Ghuman K K, Yadav S and Singh C V 2015 *J. Phys. Chem.* C **119** 6518
[41] Wassmann T, Seitsonen A P, Saitta A M, Lazzeri M and Mauri F 2008 *Phys. Rev. Lett.* **101** 096402
[42] Vazirisereshk M R *et al* 2019 *Nano Lett.* **19** 5496
[43] Zhao X, Zhang G, Wang L and Xue Q 2017 *Tribol. Lett.* **65** 64
[44] Arif T, Yadav S, Colas G, Singh C V and Filleter T 2019 *Adv. Mater. Interfaces* **6** 1901246
[45] Vazirisereshk M R, Martini A, Strubbe D A and Baykara M Z 2019 *Lubricants* **7** 57
[46] Yue Q, Shao Z, Chang S and Li J 2013 *Nanoscale Res. Lett.* **8** 425
[47] Umerbekova A, Zhang S-F and Sudheer Kumar P 2018 *Eur. Phys. J.* B **91** 214
[48] Krishtal A, Ceresoli D and Pavanello M 2015 *J. Chem. Phys.* **142** 154116
[49] Krishtal A, Sinha D, Genova A and Pavanello M 2015 *J. Phys.: Condens. Matter* **27** 183202
[50] Krishtal A and Pavanello M 2016 *J. Chem. Phys.* **144** 124118
[51] Neugebauer J 2013 *Recent Advances in Orbital-Free Density Functional Theory* ed T A Wesolowski and Y A Wang (Singapore: World Scientific)
[52] Neugebauer J 2010 *Phys. Rep.* **489** 1
[53] Neugebauer J 2009 *J. Chem. Phys.* **131** 084104
[54] Neugebauer J 2009 *ChemPhysChem* **10** 3148
[55] Neugebauer J, Curutchet C, Muñoz-Losa A and Mennucci B 2010 *J. Chem. Theory Comput.* **6** 1843
[56] König C and Neugebauer J 2011 *Phys. Chem. Chem. Phys.* **13** 10475
[57] König C, Schlüter N and Neugebauer J 2013 *J. Chem. Phys.* **138** 034104
[58] Kovyrshin A and Neugebauer J 2016 *Phys. Chem. Chem. Phys.* **18** 20955
[59] Severo Pereira Gomes A and Jacob C R 2012 *Annu. Rep. Prog. Chem.* C **108** 222
[60] Neugebauer J 2007 *J. Chem. Phys.* **126** 134116
[61] Casida M E and Wesolowski T A 2004 *Int. J. Quantum Chem.* **96** 577
[62] Neugebauer J 2008 *J. Phys. Chem.* B **112** 2207
[63] Pavanello M 2013 *J. Chem. Phys.* **138** 204118
[64] Genova A, Ceresoli D, Krishtal A, Andreussi O, DiStasio R Jr and Pavanello M 2017 *Int. J. Quantum Chem.* **117** e25401
[65] Genova A and Pavanello M 2015 *J. Phys.: Condens. Matter* **27** 495501
[66] Jacob C R and Neugebauer J 2014 *WIREs: Comput. Mol. Sci.* **4** 325
[67] Wesolowski T A, Shedge S and Zhou X 2015 *Chem. Rev.* **115** 5891
[68] Wesolowski T A 2006 *Computational Chemistry: Reviews of Current Trends* vol 10 ed J Leszczynski (Singapore: World Scientific) pp 1–82
[69] Kohn W and Sham L J 1965 *Phys. Rev.* **140** 1133
[70] Ullrich C A 2012 *Time-Dependent Density-Functional Theory: Concepts and Applications* (Oxford: Oxford University Press)
[71] Vignale G, Ullrich C A and Conti S 1997 *Phys. Rev. Lett.* **79** 4878
[72] Maitra N T, Zhang F, Cave R J and Burke K 2004 *J. Chem. Phys.* **120** 5932
[73] Maitra N T 2016 *J. Chem. Phys.* **144** 220901
[74] Neuhauser D, Pistinner S, Coomar A, Zhang X and Lu G 2011 *J. Chem. Phys.* **134** 144101
[75] Jiang K and Pavanello M 2021 *Phys. Rev.* B **103** 245102
[76] Podeszwa R, Cencek W and Szalewicz K 2012 *J. Chem. Theory Comput.* **8** 1963
[77] Misquitta A J, Jeziorski B and Szalewicz K 2003 *Phys. Rev. Lett.* **91** 033201
[78] Oliveira M J T, Komarova K, Remacle F and Verstraete M J 2019 Long-range dispersion forces between molecules subject to ultra-short optical pulses from *ab initio* calculations (arXiv:1902.01651 [physics.chem-ph])
[79] Kevorkyants R, Eshuis H and Pavanello M 2014 *J. Chem. Phys.* **141** 044127
[80] Sinha D and Pavanello M 2015 *J. Chem. Phys.* **143** 084120
[81] Dion M, Rydberg H, Schröder E, Langreth D C and Lundqvist B I 2004 *Phys. Rev. Lett.* **92** 246401
[82] Dobson J F and Gould T 2012 *J. Phys.: Condens. Matter* **24** 073201
[83] Furche F 2008 *J. Chem. Phys.* **129** 114105
[84] Shao X, Mi W and Pavanello M 2022 eDFTpy: an object-oriented platform for density embedding simulations (available at https://edftpy.rutgers.edu)

[85] Giannozzi P et al 2017 J. Phys.: Condens. Matter 29 465901
[86] Shao X, Andreussi O, Ceresoli D, Truscott M, Baczewski A, Campbell Q and Pavanello M 2022 https://gitlab.com/shaoxc/qepy QEpy: quantum ESPRESSO in python (available at https://gitlab.com/shaoxc/qepy)
[87] Qian X, Li J, Lin X and Yip S 2006 Phys. Rev. B 73 035408
[88] Luan B and Zhou R 2016 Appl. Phys. Lett. 108 131601
[89] Shao X, Umerbekova A, Jiang K and Pavanello M 2022 Supplementary data for many-body van der Waals interactions in wet MoS_2 surfaces (available on Zenodo at https://zenodo.org/record/5971766)
[90] Perdew J P, Burke K and Ernzerhof M 1996 Phys. Rev. Lett. 77 3865
[91] Constantin L A, Fabiano E, Laricchia S and Della Sala F 2011 Phys. Rev. Lett. 106 186406
[92] Garrity K F, Bennett J W, Rabe K M and Vanderbilt D 2014 Comput. Mater. Sci. 81 446
[93] Sudheer Kumar P, Genova A and Pavanello M 2017 J. Phys. Chem. Lett. 8 5077
[94] Tavernelli I 2006 Phys. Rev. B 73 094204
[95] Dreuw A and Head-Gordon M 2005 Chem. Rev. 105 4009
[96] Onida G, Reining L and Rubio A 2002 Rev. Mod. Phys. 74 601